NUCL SCI TECH (2021) 32:16
https://doi.org/10.1007/s41365-021-00851-9

Uncertainty evaluation and correlation analysis of single-particle energies in phenomenological nuclear mean field: an investigation into propagating uncertainties for independent model parameters

Zhen-Zhen Zhang[1] · Hua-Lei Wang[1] · Hai-Yan Meng[1] · Min-Liang Liu[2]

Received: 28 October 2020 / Revised: 4 December 2020 / Accepted: 4 December 2020 / Published online: 15 February 2021

Abstract Based on the Monte Carlo approach and conventional error analysis theory, taking the heaviest doubly magic nucleus ^{208}Pb as an example, we first evaluate the propagated uncertainties of universal potential parameters for three typical types of single-particle energy in the phenomenological Woods–Saxon mean field. Accepting the Woods–Saxon modeling with uncorrelated model parameters, we found that the standard deviations of single-particle energy obtained through the Monte Carlo simulation and the error propagation rules are in good agreement. It seems that the energy uncertainty of the single-particle levels regularly evoluate with certain quantum numbers to a large extent for the given parameter uncertainties. Further, the correlation properties of the single-particle levels within the domain of input parameter uncertainties are statistically analyzed, for example, with the aid of Pearson's correlation coefficients. It was found that a positive, negative, or unrelated relationship may appear between two selected single-particle levels, which will be extremely helpful for evaluating the theoretical uncertainty related to the single-particle levels (e.g., K isomer) in nuclear structural calculations.

Keywords Uncertainty propagation · Correlation effect · Woods–Saxon potential

1 Introduction

The fundamental theory of strong interactions is quantum chromodynamics [1]. As a final goal, all phenomena in nuclear structures are expected to be derived from the interactions of quarks and gluons. To date, although the density functional theory has been applied, attaining such a goal remains difficult. In practice, to make the task tractable and more physically intuitive, numerous simplifications are usually made in theoretical nuclei modeling. As is well known, the first approximation is the use of the concept of nucleons and their interactions, which has been adopted in nearly all contemporary theories of a nuclear structure. Further, mean-field approximations and nucleon effective interactions are proposed, respectively, owing to the difficulty of solving the many-body problem and the complexity of the nucleon-nucleon interactions. In general, theoretical models for a nuclear structure can be grouped into ab initio methods, mean-field theories, and shell model theories, among others ([2] and the references therein).

Nuclear mean-field theories include phenomenological or empirical [3–6] (e.g., the nuclear potentials of Woods–Saxon and Nilsson types) and self-consistent [7–9] (e.g., numerous variants related to the Hartree–Fock approximation) approaches, which assume that all nucleons move independently along their orbits. In this type of nuclear theory, the underlying element contributing to the high

This work was supported by the National Natural Science Foundation of China (No. 11975209), the Physics Research and Development Program of Zhengzhou University (No. 32410017), and the Project of Youth Backbone Teachers of Colleges and Universities of Henan Province (No. 2017GGJS008). Some of the calculations were conducted at the National Supercomputing Center in Zhengzhou.

✉ Hua-Lei Wang
wanghualei@zzu.edu.cn

[1] School of Physics and Microelectronics, Zhengzhou University, Zhengzhou 450001, China

[2] Institute of Modern Physics, Chinese Academy of Sciences, Lanzhou 730000, China

quality of the theoretical calculations is the reliable mean-field single-particle energies, which sensitively depend on the corresponding Hamiltonian modeling and model parameters. For a defined mathematical model, the sampling (selection) and quality of the experimental data will determine the resulting optimal parameter set and its quality. In principle, this can be achieved through standard statistical fitting procedures, such as a least squares and χ^2 fitting [10–13]. The physical quantity can then be computed using the optimal parameters. However, in the language of statistics, an overfitting (underfitting) may appear if the model contains more (less) parameters. For instance, it was pointed out that the so-called realistic model interactions appear most of the time to be strongly over-parameterized [14]. Therefore, there will remain uncertainties originating from the size of the sample database, errors in the experimental data, a limited reliability of the model, and the numerical method used [15]. In recent years, model prediction capacities and estimations of theoretical uncertainties have been of significant interest in many subfields of physics and technological applications [16–20]. Even so, it was pointed out that model predictions without properly quantified theoretical errors will have an extremely limited utility [23].

The phenomenological mean field, for example, the realistic Woods–Saxon potential, has been used for many decades in nuclear physics and is considered to have an extremely high predictive power for single-nucleon energies, whereas related computing algorithms remain relatively simple. The model uncertainties and predictive power of a spherically symmetric Woods–Saxon mean field have been investigated [14], with particular attention paid to issues of parameter adjustment and parametric correlations. Prior to this study, based on a one-body Hamiltonian with a phenomenological mean field of the deformed Woods–Saxon type, some studies [24–27] have been conducted on different isotopes within the framework of the macroscopic-microscopic model [28, 29] and cranking approximation [30, 31], focusing on different ground-state and high-spin nuclear properties. The main interest of our present study is not the fitting of the new parameters, the parameter uncertainties, or an investigation of parameter correlations, but rather the propagation of the reasonably given parameter uncertainties and the statistical correlation properties of the calculated single-particle levels within the domain of the input parameter uncertainties using the same Woods–Saxon Hamiltonian. Thus far, such a systematic study is scarce and meaningful, particularly for the theoretical calculations (e.g., K isomer predictions) that depend strongly on single-particle levels. As is well known, the single-particle levels are independent (which means that the eigenfunctions of the Hamiltonian operator are orthogonal for different levels) in the mean-field approximation without the inclusion of the residual interaction. The wording of the 'correlation properties' for the levels may be considered unsuitable, and may even be seriously misunderstood by general readers. Therefore, it should be noted that the correlation property mentioned here indicates the statistical correlation (rather than something else, e.g., the correlation between the spin partners $j = l \pm 1/2$) used to reveal the linear relationship of any two levels within the small domains related to their energy uncertainties. The calculated single-particle levels have a probability distribution (namely, the property of a stochastic quantity) after considering the uncertainty propagation of the model parameters. That is, each calculated single-particle level will have a fixed value when calculating at a fixed mean field without considering the model parameter uncertainties, whereas it will possess a stochastic value near its 'fixed' value once the model parameter uncertainties are considered. As one of the aims of the present study, we investigate the correlations between these stochastic values rather than the 'relationships' of those 'fixed' values. It should also be noted that, as an example for conducting the present investigation, we first accept the Woods–Saxon modeling with independent model parameters and then take the doubly magic nucleus of ^{208}Pb (which has always been regarded as a benchmark in studies on the nuclear structure). The parameter uncertainties for the Woods–Saxon potential, and even the parameter correlations, have been estimated based on the maximum likelihood and Monte Carlo methods [14, 19].

The remainder of the paper is organized as follows. In Sect. 2, we briefly introduce our theoretical framework on the single-particle Hamiltonian, Monte Carlo method, and propagation of the uncertainty and Pearson's product-moment correlation. Section 3 presents our results and a discussion of the evaluation of universal potential parameters, the generation of pseudo data, uncertainties of single-particle energies, and the correlation effects between them. Finally, we provide some concluding remarks in Sect. 4.

2 Theoretical framework

Given that our main goal is the uncertainty evolution of single-particle levels and the assessment of correlations among them owing to the error propagation of the model parameters rather than the Hamiltonian modeling, the fitting of the parameters or other physics issues, we review some related points that are helpful for general readers, although there are numerous related references for each aspect.

2.1 Woods–Saxon single-particle Hamiltonian

The single-particle levels and wave functions are calculated by numerically solving the stationary Schrödinger equation with an average nuclear field of the Woods–Saxon type. The single-particle Hamiltonian for this equation is given by [5, 6]

$$H_{\mathrm{WS}} = -\frac{\hbar^2}{2m}\nabla^2 + V_{\mathrm{cent}}(\vec{r};\hat{\beta}) + V_{\mathrm{so}}(\vec{r},\vec{p},\vec{s};\hat{\beta}) + \frac{1}{2}(1+\tau_3)V_{\mathrm{Coul}}(\vec{r},\hat{\beta}), \tag{1}$$

where the Coulomb potential $V_{\mathrm{Coul}}(\vec{r},\hat{\beta})$, defined as a classical electrostatic potential of a uniformly charged drop is added for protons. The first part on the right side of Eq. (1) is the kinetic energy term. The central part of the Woods–Saxon potential, which mainly controls the number of levels in the potential well is [6]

$$V_{\mathrm{cent}}(\vec{r},\hat{\beta}) = \frac{V_0[1 \pm \kappa(N-Z)/(N+Z)]}{1+\exp[\mathrm{dist}_{\Sigma}(\vec{r},\hat{\beta})/a]}, \tag{2}$$

where the plus and minus signs hold for protons and neutrons, respectively, and a is the diffuseness parameter of the nuclear surface. The spin-orbit potential, which can strongly affect the level order, is defined as follows:

$$V_{\mathrm{so}}(\vec{r},\vec{p},\vec{s};\hat{\beta}) = -\lambda\left[\frac{\hbar}{2mc}\right]^2 \left\{\nabla \frac{V_0[1 \pm \kappa(N-Z)/(N+Z)]}{1+\exp[\mathrm{dist}_{\Sigma_{\mathrm{so}}}(\vec{r},\hat{\beta})/a_{\mathrm{so}}]}\right\} \times \vec{p}\cdot\vec{s}, \tag{3}$$

where λ denotes the strength parameter of the effective spin-orbit force acting on the individual nucleons. In Eq. (2), the term $\mathrm{dis}_{\Sigma}(\vec{r},\hat{\beta})$ indicates the distance of a point $\vec{r}$ from the nuclear surface, Σ. The nuclear surface is parameterized in terms of the multipole expansion of spherical harmonics $\mathrm{Y}_{\lambda\mu}(\theta,\phi)$, namely,

$$\Sigma : R(\theta,\phi) = r_0 A^{1/3} c(\hat{\beta})\left[1 + \sum_{\lambda}\sum_{\mu=-\lambda}^{+\lambda} \alpha_{\lambda\mu}\mathrm{Y}^*_{\lambda\mu}(\theta,\phi)\right], \tag{4}$$

where the function $c(\hat{\beta})$ ensures the conservation of the nuclear volume with a change in the nuclear shape, and $\hat{\beta}$ denotes the set of all considered deformation parameters. This is similar in Eq. 3, although the new surface Σ_{so} needs to be calculated using different radius parameters.

Based on the Woods–Saxon Hamiltonian as mentioned above, the Hamiltonian matrix is calculated using the axially deformed harmonic-oscillator basis in the cylindrical coordinate system with the principal quantum number $N \leqslant 12$ and 14 or protons and neutrons, respectively. Then, after a diagonalization procedure, the single-particle levels and their wave functions can be obtained. It is shown in the present study that the calculated single-particle levels with such a basis cutoff will be sufficiently stable with respect to a possible basis enlargement. Of course, one can see that for a given (Z, N) nucleus, the calculated energy levels $\{e\}_{\pi,\nu}$ depend on two sets of six free parameters:

$$\{V^{\mathrm{c}}, r^{\mathrm{c}}, a^{\mathrm{c}}, \lambda^{\mathrm{so}}, r^{\mathrm{so}}, a^{\mathrm{so}}\}_{\pi,\nu}, \tag{5}$$

one set with the symbol π for protons, and the other set with ν for neutrons; in addition, the superscripts 'c' and 'so' denote the abbreviations for 'central' and 'spin-orbit', respectively.

For convenience, we define the parameter set $\{p\} \equiv \{p_1,p_2,p_3,p_4,p_5,p_6\}$, which is associated with the original as follows:

$$\{p_1,p_2,p_3,p_4,p_5,p_6\}_{\pi,\nu} \rightarrow \{V^{\mathrm{c}}, r^{\mathrm{c}}, a^{\mathrm{c}}, \lambda^{\mathrm{so}}, r^{\mathrm{so}}, a^{\mathrm{so}}\}_{\pi,\nu}. \tag{6}$$

Further, following the notation of [32, 33], we can denote a point in such a parameter space by $\mathbf{p} = (p_1,p_2,p_3,p_4,p_5,p_6)$. According to the inverse problem theory, the model parameters are usually determined by fitting to a set of observables within a selected sample (e.g., the available sample database of the experimental single-particle levels). For a given mathematical model, for example, accepting the Woods–Saxon Hamiltonian with free parameters, the optimum parametrization $\mathbf{p}^{\mathrm{o}}$ can usually be obtained with a least-squares fitting using a global quality measure [33–35],

$$\chi^2(\mathbf{p}) = \sum_{n=1}^{N}\left(\frac{O_n^{(\mathrm{th})}(\mathbf{p}) - O_n^{(\mathrm{exp})}}{\Delta O_n}\right)^2 \tag{7}$$

where 'th' indicates the calculated values, 'exp' represents the experimental data, and ΔO indicates the adopted errors, which generally contain the contributions from both experimental and theoretical aspects. Note that the definition of the objective function χ^2 is the standard, and several powerful techniques for finding its minimum value have already been developed. The universal parameter set used in the present investigation is indeed one such 'optimal' parameter set. Having determined $\mathbf{p}^{\mathrm{o}}$, in principle, any physics quantity, for example, the single-particle level e_i, can be computed at $e_i(\mathbf{p}^{\mathrm{o}})$. From this point, we can to an extent regard the calculated energy level e_i as a function of the corresponding parameter set $\{p\}$, namely,

$$e_i = e_i(p_1,p_2,p_3,p_4,p_5,p_6). \tag{8}$$

There is no doubt that the $\mathbf{p}$ value depends on the size and quality of the selected sample database. In fact, the functional relationship of Eq. (8) expresses not only a physical

law but also the measured and calculated processes. All uncertainties during the physical modeling, experimental measurement, and theoretical calculation may lead to uncertainty of the **p** value. By contrast, the uncertainty of the **p** value will propagate to the results of the calculations.

2.2 Uncertainty estimation of single-particle levels

By reasonably assuming that input parameters $\{p\}$ are Gaussian random variables, we will be able to estimate the uncertainties of the single-particle levels owing to the input uncertainties of the potential parameters using the conventional analysis method [36–38] (e.g., the formula of uncertainty propagation) and the Monte Carlo method [39–43]. Based on the functional relationship of Eq. (8) and the uncertainty propagation formula, the uncertainty of the ith single-particle level e_i with random and uncorrelated inputs can be given analytically by the following:

$$\sigma_{e_i} = \sqrt{\sum_{j=1}^{6}\left(\frac{\partial e_i}{\partial p_j}\right)^2 \cdot \sigma_{p_j}^2}, \tag{9}$$

where σ_{p_j} is the standard deviation of the input parameter p_j; in addition, the partial derivative $\partial e_i/\partial p_j$ is usually called the sensitivity coefficient, which provide the effect of the corresponding input parameter on the final result. Note that both the linearity of the function (at least, near the calculated point p_j) and the 'small' uncertainty of the input parameter are prerequisites of a conventional uncertainty estimation method. However, there is no such limitation for the Monte Carlo simulation method, which can handle both small and large uncertainties in the input quantities. Moreover, the Monte Carlo simulation, which can be generally defined as the process of replication of the 'real' world, has the ability to account for partial correlation effects for the input parameters. It is also convenient to study the correlation effect, e.g., between two Gaussian-distributed variables, whereas the conventional method cannot do so.

As known in such a simulation, the availability of high-quality Gaussian random numbers is important. Generally speaking, the realization of a Gaussian-random-number generator can adopt both software and hardware methods. The former has limited speed and poor real-time characteristics, whereas the latter (which is based on digital devices) is not only fast, with real-time implementation, but also has good flexibility and accuracy. At present, the majority of the frequently used digital methods for generating Gaussian random variables are based on transformations from uniform random variables. Popular methods, for instance, include the Ziggurat method [44], an inversion method [45], the Wallace method [46], and the Box–Muller method [47–50]. In the present study, we realize hardware Gaussian random number generators using the Box–Muller algorithm. In other words, taking each value p_j^{o} of the universal parameter set $\{p_1^{\mathrm{o}}, p_2^{\mathrm{o}}, p_3^{\mathrm{o}}, p_4^{\mathrm{o}}, p_5^{\mathrm{o}}, p_6^{\mathrm{o}}\}$ as the corresponding mean value, one can generate the random and uncorrelated input parameter p_j following a normal distribution $N(p_j^{\mathrm{o}}, \sigma_{p_j})$. With a large sample of input parameters, the uncertainties of single-particle levels can be estimated. For instance, considering the uncertainty of one input parameter p_j and keeping other universal values unchanged, the variance of the calculated e_i can be given by the following:

$$\sigma_{e_i}^2 = \frac{1}{N-1}\sum_{k=1}^{N}[e_i(p_{jk}) - e_i(p_j^{\mathrm{o}})]^2, \tag{10}$$

where the sampling number N should be chosen to be sufficiently large (e.g., 10,000 or more). Similar calculations can be conducted when the uncertainties of two or more input parameters are opened. Therefore, we will be able to investigate the effects of the uncertainties of different input parameters and their combinations on the uncertainties of single-particle levels.

2.3 Pearson product moment correlation

The single-particle levels with certain uncertainties can usually be regarded as the input variables in further nuclear mean-field calculations, for example, K isomeric calculations. In this case, to evaluate further theoretical predictions, it will be extremely useful to know both the uncertainties and correlation properties of the single-particle levels. As a simple example, the energy uncertainty of one-particle one-hole ($1p1h$) excitation is directly related to two corresponding single-particle levels to a large extent. We can arbitrarily regard the excitation energy E_{1p1h} as a function of two single-particle levels e_1 and e_2 with the standard deviations σ_{e_1} and σ_{e_2}, respectively, namely,

$$E_{1p1h}^{*} = f(e_1, e_2). \tag{11}$$

Regardless of whether e_1 and e_2 are independent, the standard uncertainty of such an excited state can be written as [51]

$$\sigma_{E_{1p1h}^{*}} = \sqrt{\left(\frac{\partial f}{\partial e_1}\right)^2\sigma_{e_1}^2 + \left(\frac{\partial f}{\partial e_2}\right)^2\sigma_{e_2}^2 + 2\frac{\partial f}{\partial e_1}\frac{\partial f}{\partial e_2}\rho(e_1,e_2)\sigma_{e_1}\sigma_{e_2}}, \tag{12}$$

where the quantity $\rho(e_1,e_2)$ is the Pearson's correlation coefficient, which is given by [52, 53]

$$\rho(e_1, e_2) = \frac{cov(e_1, e_2)}{\sigma_{e_1}\sigma_{e_2}}. \quad (13)$$

Such a cross-correlation coefficient measures the strength and direction of a linear relationship between two variables, for example, e_1 and e_2. The greater the absolute value of the correlation coefficient, the stronger the relationship. The extreme values of -1 and 1 indicate a perfectly linear relationship where a change in one variable is accompanied by a perfectly consistent change in the other. For these two cases, all of the data points fall on a line. A zero coefficient represents a non-linear relationship. That is, as one variable increases, there is no tendency in the other variable to either increase or decrease. When the cross-correlation coefficient is between 0 and +1/-1, there will be a relationship, but not all points fall on a line. The sign of the correlation coefficient represents the direction of the linear relationship. Positive coefficients indicate that when the value of one variable increases, the value of the other variable also tends to increase. Positive relationships produce an upward slope on a scatterplot. Negative coefficients indicate that when the value of one variable increases, the value of the other variable tends to decrease. Correspondingly, negative relationships produce a downward slope. It should be noted that the Pearson's correlation coefficient, which measures only the linear relationships between two variables, will not detect a curvilinear relationship. For instance, when the scatterplot of two variables shows a symmetric distribution, a relationship may exist, but the correlation coefficient is zero.

3 Results and discussion

3.1 Evaluation of Woods–Saxon potential parameters

In the phenomenological nuclear mean field, the realistic Woods–Saxon potential has shown certain advantages and is still widely used. For instance, it provides a good description of not only the ground-state properties but also the excited-state properties of the nuclei. Currently, many authors are still working on different issues with the Woods–Saxon potential. Such a simple nuclear mean field has been successfully applied to explain and predict the nuclear equilibrium deformations, the high-K isomer, the nucleon binding energies, the fission barriers, numerous single-particle effects for super-deformed and fast rotating nuclei, and so on. As shown in Table 1, there exist various parametrizations of the Woods–Saxon potential ([6] and references therein), which are usually obtained by fitting the available single-particle data (or part of the data, namely, one of the sub-databases) or other observables. Indeed, based on the same mathematical modeling and different sample databases and sub-databases, different parameter sets can be obtained. It can be seen that these parameter sets are somewhat different, even rather different for some quantities among them. Correspondingly, the different parameter sets are suitable for a certain nuclear mass region. Occasionally, the difference in the corresponding quantity (e.g., single-particle energies) calculated theoretically using different parameter sets is referred to as a model discrepancy, which can be evaluated by using different models and/or different parameter sets. The universal parameter set of the Woods–Saxon potential is one of the most common parameter sets. In principle, it can be used for the 'global' calculation of the nuclei. In the present study, we conducted our investigation based on the universal parameter set.

To evaluate the universal potential parameters, Fig. 1a shows the discrepancies ΔE ($\equiv e_i^{\text{theo.}} - e_i^{\text{exp.}}$) of the calculated single-particle energies from the available data (e.g., eight spherical nuclei [54, 55]: ^{16}O,^{40}Ca,^{48}Ca, ^{56}Ni,^{90}Zr,^{132}Sn,^{146}Gd and ^{208}Pb). The discrepancies show us that the single-particle levels generated by the universal parameters, in fact, cannot agree with the data very well (i.e., similar to the mass calculation [56], the quest for some possibly missing interactions and 'better' mathematical modeling will never cease). Moreover, most of the values are smaller or larger than the data. For instance, as shown, a systematic overestimation and underestimation for protons and neutrons exist, respectively, particularly in lighter nuclei. To see the statistical properties of the parameters, the percentage difference, $PD(p_j)$, of the model parameter p_j (as an example, $j = 1$ herein) extracted from the experimental data is presented in Fig. 1b, which is defined as follows:

$$PD(p_j) = \frac{p_j^{\text{b}} - p_j^{\text{o}}}{\frac{p_j^{\text{b}} + p_j^{\text{o}}}{2}} \times 100\%, \quad (14)$$

where p_j^{o} indicates the jth 'optimal' (universal) value of the $\{p\}$ parameters, and the p_j^{b} parameter denotes the so-called best value that can be obtained based on the following method. For a certain model parameter, for example, the potential depth p_1 (namely, V_0) of the Woods–Saxon parameters, we calculate the corresponding single-particle energies of a given nucleus by varying the value of this parameter p_1 around its optimal value p_1^{o} and keeping other parameters with universal values unchanged. If the discrepancy of the calculated single-particle energy for a certain nucleus from the corresponding experimental data equals zero, the "best" value p_1^{b} of this parameter p_1 for this nucleus is therefore obtained. In principle, for a large

Table 1 Various parameter sets for Woods–Saxon potential

Parameter		V_0 (MeV)	r_0^{c} (fm),	a_0^{c} (fm)	λ	r_0^{so} (fm)	a_0^{so} (fm)
Wahlborn [57]		51.0	1.27	0.67	32.0	1.27	0.67
Rost [58]	n	49.6	1.347	0.7	31.5	1.280	0.7
	p		1.275		17.8	0.932	
Chepurnov [59]		53.3	1.24	0.63	$23.8 \cdot (1+2I)$	1.24	0.63
New [60]	n	49.6	1.347	0.7	*	*	0.7
	p		1.275		*	*	
Universal [6]	n	49.6	1.347	0.7	35.0	1.31	0.7
	p		1.275		36.0	1.32	
Optimized [61]	n	49.6	1.347	0.7	36.0	1.30	0.7
	p		1.275				
Cranking [62, 63]		53.754	1.19	0.637	29.494	1.19	0.637

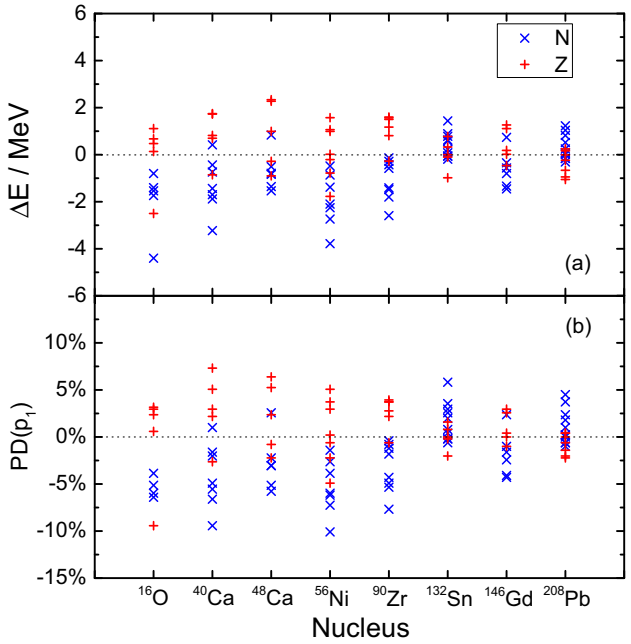

Fig. 1 (Color online) **a** Discrepancies between the available experimental data and the calculated single-particle energies using the Woods–Saxon Universal parameter set for even-even nuclei ^{16}O, ^{40}Ca,^{48}Ca, ^{56}Ni,^{90}Zr,^{132}Sn,^{146}Gd and ^{208}Pb. The data were taken from [54, 55]. **b** Percentage differences between the 'best' and 'optimal' p_1 (namely, V_0) parameters. See the text for more details

sample, we can extract the standard deviation σ_{p_1} with a confidence level of 68.3% for the parameter p_1. From Fig. 1b, it was found that the percentage differences distribute between $\pm 10\%$. Similar distributions exist for other potential parameters as well. Based on these statistical properties and some previous studies (for example, [16, 19]), we can evaluate the uncertainty of Woods–Saxon parameters to an extent. Furthermore, we will be able to temporarily provide the standard deviations $\{\sigma_p\} \equiv \{\sigma_{p_1}, \sigma_{p_2}, \sigma_{p_3}, \sigma_{p_4}, \sigma_{p_5}, \sigma_{p_6}\}$ for the parameters $\{p\}$ within reasonable domains, taking the universal parameters $\{p_1^{\mathrm{o}}, p_2^{\mathrm{o}}, p_3^{\mathrm{o}}, p_4^{\mathrm{o}}, p_5^{\mathrm{o}}, p_6^{\mathrm{o}}\}$ as the corresponding mean values.

3.2 Producing pseudo-data of potential parameters

Based on the given mean values $\{p^{\mathrm{o}}\}$ and the corresponding standard deviations $\{\sigma_p\}$, the Gaussian-distributed random sets $\{p\}$ can, in principle, be numerically generated in the spirit of the Monte Carlo approach. Considering the uncertainty estimations of the Woods–Saxon parameters and the sensitivity coefficients of single-particle levels, in practice, we use a set of percentage coefficients

$$\{c\} \equiv \{c_1, c_2, c_3, c_4, c_5, c_6\} = \{0.1\%, 0.1\%, 1\%, 3\%, 1\%, 10\%\}$$

to calibrate the standard deviations $\{\sigma_p\}$ during the calculations. That is, the standard deviations are given by the following:

$$\begin{pmatrix} \sigma_{p_1} \\ \sigma_{p_2} \\ \sigma_{p_3} \\ \sigma_{p_4} \\ \sigma_{p_5} \\ \sigma_{p_6} \end{pmatrix} = \begin{pmatrix} c_1 & c_2 & c_3 & c_4 & c_5 & c_6 \end{pmatrix} \begin{pmatrix} p_1^{\mathrm{o}} \\ p_2^{\mathrm{o}} \\ p_3^{\mathrm{o}} \\ p_4^{\mathrm{o}} \\ p_5^{\mathrm{o}} \\ p_6^{\mathrm{o}} \end{pmatrix}. \qquad (15)$$

Such a set σ_p may deviate from the 'true' values to a certain extent but does not affect the conclusion of our investigation because the values lie within the reasonable domains. Moreover, the strong overlaps of the 'peaks' of single-particle levels can be avoided (as shown below). We conducted Woods–Saxon single-particle-level calculations with 10,000 samples for $\{p\}$, which is sufficient large to suppress the error coming from stochastic choices. To show the quality of the normally distributed random quantities $\{p\}$, Fig. 2 presents the two-dimensional scatter plots related to the six Woods–Saxon parameter samplings of neutrons, together with the corresponding correlation

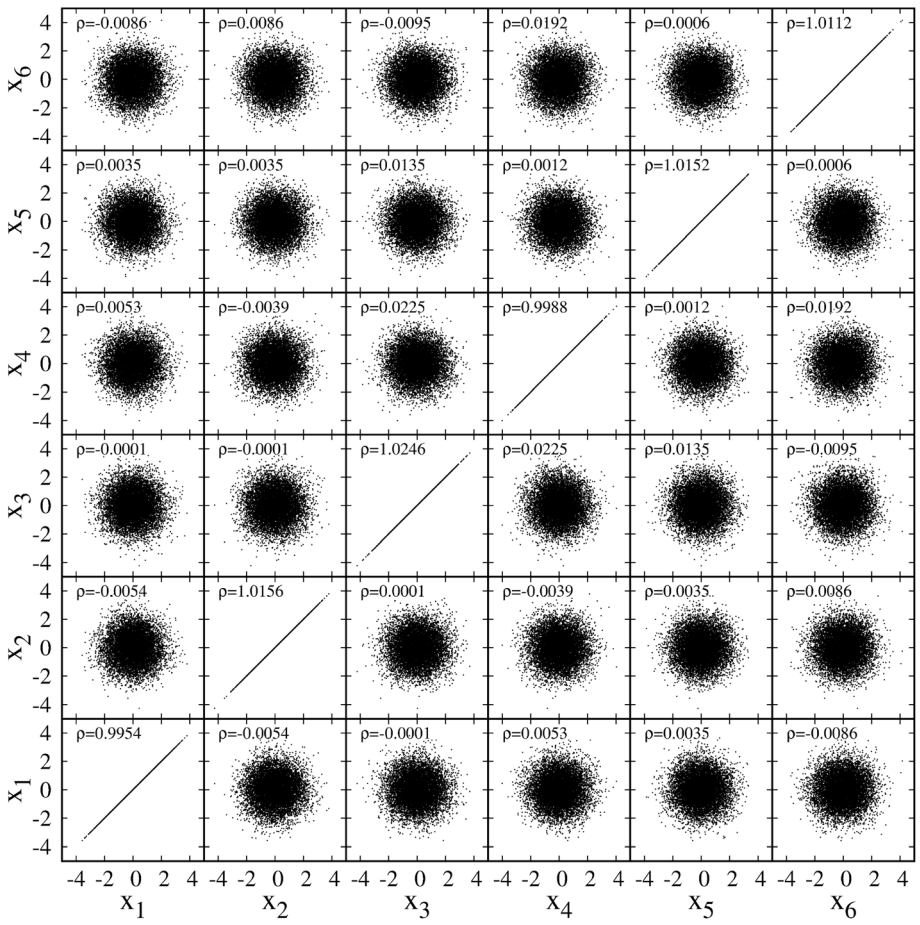

Fig. 2 Two-dimensional scatter plots, together with their corresponding correlation coefficients, between six independent WS model parameters

coefficients. Note that this is similar for the protons as well. For comparison, the normal distribution $N(p_i^{\mathrm{o}}, \sigma_{p_i})$ is transformed into the standard normal distribution $N(0, 1)$ by defining the dimensionless parameter $x_i = (p_i - p_i^{\mathrm{o}})/\sigma_{p_i}$ in Fig. 2. The Gaussian-distributed and independent properties of these parameters can be seen. In addition, the calculated skewness and kurtosis values are zero, as expected, indicating Gaussian-type distributions.

3.3 Uncertainties of single-particle energies

With the sampling $\{p\}$, the uncertainties of the single-particle energies will be able to be precisely evaluated. Indeed, this is an advantage of the Monte Carlo method. For convenience, using a similar $\gamma - \gamma$ coincidence technique, which is widely applied for experimentally deducing the nuclear level scheme, we construct a level-level coincidence matrix (namely, a two-dimensional histogram). Each axis of the matrix corresponds to the energy of the calculated single-particle levels. The matrix has channel dimensions of 4096×4096, with an energy calibration of 10 keV/channel. Such a matrix provides an energy range of -40.96 to 0.00 MeV, covering the range of the single-particle energies (e.g., all bounded ones for neutrons) considered. By using the gated spectra on different level-level matrice, the peak distributions of single-particle levels and even their correlation properties can be conveniently analyzed under different conditions.

It is well known that there are three typical types of single-particle levels during the evolution of the nuclear models (for instance, from the harmonic oscillator model, adding strong spin-orbit coupling to obtain the shell model, and an axial deformation to provide the collective model). In this study, we use a more realistic Woods–Saxon potential (lying between the harmonic oscillator potential and the finite square well) to produce these three types of single-particle levels and study their energy uncertainties originating from the model parameters. Similar to the parameter space $(p_1, p_2, p_3, p_4, p_5, p_6)$, let us define a correspondingly six-dimensional 'switch' space $(s_1, s_2, s_3, s_4, s_5, s_6)$, where $s_i = 0$ or 1 (for $i = 1, 2, \cdots, 6$). Moreover, if $s_i = 0$, the universal parameter p_i^{o} is always adopted (i.e., the standard deviation σ_{p_i} is not used). For $s_i = 1$, this indicates that the sampling p_i value is adopted (i.e., the parameter σ_{p_i} is opened). Clearly, we can evaluate the effects of different parameter uncertainties and their

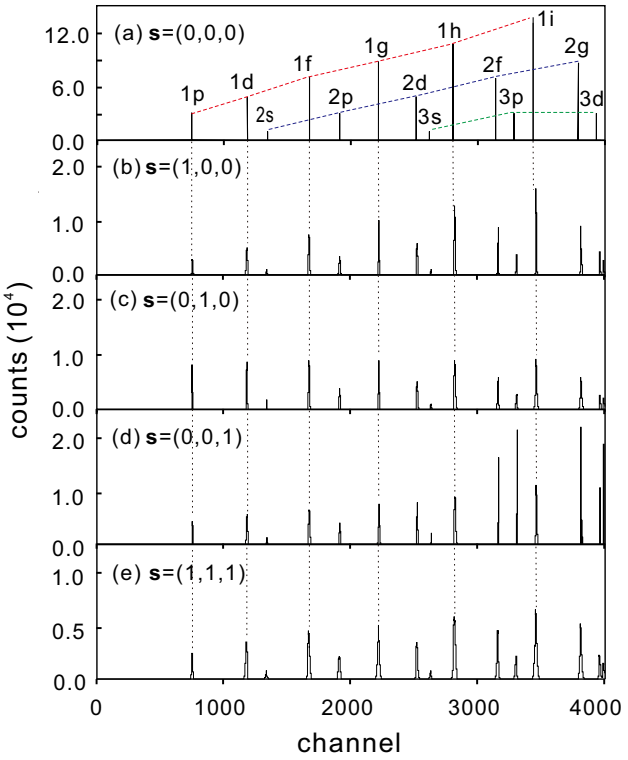

Fig. 3 Calculated single-neutron levels labeled $\{nl\}$ in ^{208}Pb (gated at the $1s$ level). The dotted lines are provided to guide the eye. See the text for further details

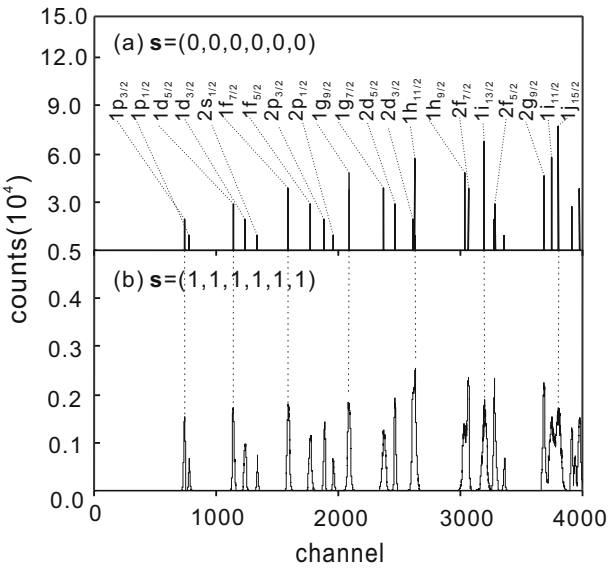

Fig. 4 (Color online) Similar to Fig. 3, although spin-orbit coupling is considered (gated at the $1s_{1/2}$ level)

combinations on single-particle levels by calculating at different points $\mathbf{s} = (s_1, s_2, s_3, s_4, s_5, s_6)$.

In Fig. 3, we show the spherical single-particle levels (labeled as $\{nl\}$ quantum numbers) calculated using the Woods–Saxon potential without the inclusion of spin-orbit coupling. Note that in the spectroscopic notation, the bounded states under angular momentum with $l = 0, 1, 2, 3, 4, 5, \cdots$ are indicated with the letter $s, p, d, f, g, h, \cdots$, respectively. The projection spectra at different $\mathbf{s}$ points are obtained by gating at the $1s$ level. Figure 4 shows the second type of single-particle levels (labeled as $\{nlj\}$) calculated at two $\mathbf{s}$ points using the spherically Woods–Saxon potential with the spin-orbit part. In this case, the l orbital is split into two $j = l \pm \frac{1}{2}$ substates. Similar to Fig. 4, in Fig. 5, we show the deformed Woods–Saxon single-particle levels (labeled as $\{\Omega[Nn_z\Lambda]\}$, the so-called Nilsson quantum numbers) calculated at $\beta_2 = 0.1$, which is an arbitrarily selected axial deformation value. In Fig. 5, the peak heights of the deformed single-particle levels are all the same, with a sampling value of 10,000, because the two-fold degenerate levels $\{\Omega[Nn_z\Lambda]\}$ are no longer degenerate. However, the levels labeled $\{nl\}$ and $\{nlj\}$ have $(2n + 1)$- and $(j + \frac{1}{2})$-fold degeneracies, respectively, owing to the spherical symmetry of the Woods–Saxon potential. As shown in Figs. 3a and 4a, the counts dividing by 10,000 indicate the degrees of degeneracy of the corresponding levels. Based on these gated spectra at different $\mathbf{s}$ points, we can analyze the distributed properties of the single-particle levels without a strong overlap. For instance, it is convenient to fit the distributions in Figs. 3 and 4, whereas it is difficult to do so in the right part of Fig. 5 because the distributions strongly overlap.

In Fig. 6a, as an example, we show the uncertainty evolution of the selected spherical $i_{13/2}$ level as an increasing number of uncertainty parameters are revealed. It can be seen that the energy uncertainty of this level increases with increasing '1' in the 'switch' space. The results of the Gaussian fits to the peaks at the $\mathbf{s} = (1, 0, 0, 0, 0, 0)$ and (1, 1, 1, 1, 1, 1) points are presented in Fig. 6b, including the standard deviations and full width at half maximum (FWHM). The FWHM is a parameter commonly used to describe the width of a "bump," e.g., on a function curve given by the distance between points on the curve at which the function reaches half its maximum value. The FWHM can be used to describe the width of any distribution. For a normal distribution $N(\mu, \sigma)$, its FWHM is $2\sqrt{2\ln 2}\ \sigma (\approx 2.3548\sigma)$. In principle, we can extract the standard deviation σ_{e_i} for each single-particle level e_i and further find the possible evolutionary law. It was found that, in practice, the correct fitting will be rather difficult to be achieved once the peak is not 'pure', although we try to limit the amplitudes of the given standard deviations $\{\sigma_p\}$.

Fortunately, we found that the single-particle energy e_i depends linearly on the potential parameters within the uncertainty domain near the universal parameters. That is,

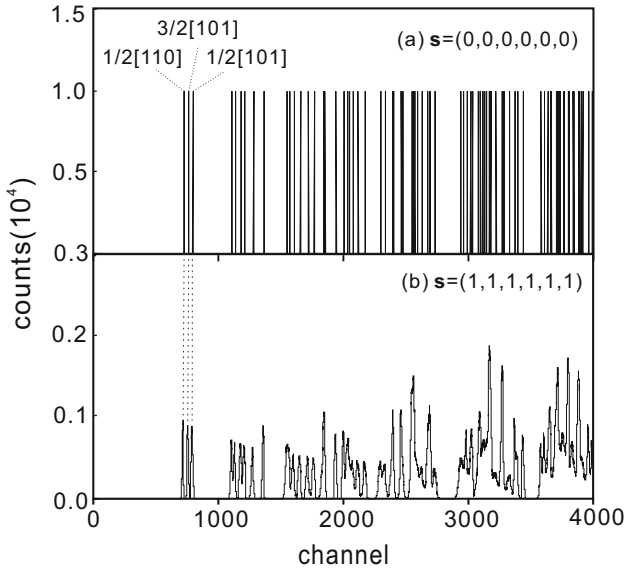

Fig. 5 Similar to Fig. 4, although the axial deformation is added (gated at the 1/2[100] level). Note that only the first three $\{\Omega[Nn_z\Lambda]\}$ quantum numbers are given owing to space limitations

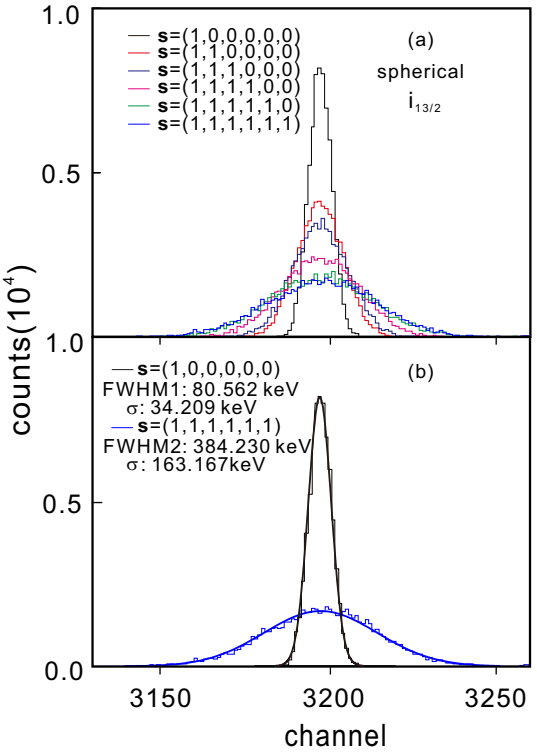

Fig. 6 (Color online) **a** Distributions of the spherical $i_{13/2}$ level calculated at different $\mathbf{s} = (s_1, s_2, s_3, s_4, s_5, s_6)$ points. **b** The Gaussian fits to the distributions at the $\mathbf{s} = (1, 0, 0, 0, 0, 0)$ and (1, 1, 1, 1, 1, 1) points

it is sufficient to use the first-order Taylor approximation in Eq. (8), which means that we can approximate the function $e_i = e_i(p_j)$ using its tangent line at the p_j^{o} point. Therefore, we can analytically calculate the energy uncertainty σ_{e_i} according to Eq. (8). The partial derivatives (sensitivity coefficients) of the single-particle energies e_i with respect to the potential parameters $\{p\}$ at $\{p^{\mathrm{o}}\}$ can be numerically calculated using the finite-difference formula:

$$\frac{\partial e_i}{\partial p_j} \simeq \frac{e_i(p_j^+) - e_i(p_j^-)}{p_j^+ - p_j^-}, \tag{16}$$

with values of p_j^+ and p_j^- suitably close to p_j^{o}. For convenience, we define an adjusted sensitivity coefficient as follows:

$$\partial_j e_i \equiv \frac{\partial e_i}{\partial p_j}\sigma_{p_j}. \tag{17}$$

By giving a set of suitable $\{\sigma_p\}$, the adjusted sensitivity coefficients $\{\partial e_i\} \equiv \{\partial_1 e_i, \partial_2 e_i, \partial_3 e_i, \partial_4 e_i, \partial_5 e_i, \partial_6 e_i\}$ will have a similar order of magnitude. Figure 7 shows the adjusted sensitivity coefficients for the three types of calculated neutron single-particle levels labeled, respectively, by $\{nl\}$, $\{nlj\}$, and $\{\Omega[Nn_z\Lambda]\}$ in ^{208}Pb. From this figure, it can be seen that the adjusted sensitivity coefficients show us regular evolution trends. In particular, the spectrum envelopes, e.g., in Fig. 7g–i and m–o, show different but interesting properties. It will be meaningful to reveal the physics behind them. Based on these sensitivity coefficients and the standard deviations of these model parameters or their combinations (namely, the adjusted sensitivity coefficients), we can calculate the energy uncertainty e_i analytically. Indeed, for the $i_{13/2}$ level, the analytical result coincides with the fitting value of the peak generated using the Monte-Carlo method. The typical error between the calculated and fitted values is less than 3%.

Based on the above method, we analytically calculate the overall uncertainties of the three levels mentioned above for both neutrons and protons in ^{208}Pb. In the calculations, all parameter uncertainties are taken into account, which indicates that calculations are conducted at the $\mathbf{s} = (1, 1, 1)$ point for $\{nl\}$ levels and at the $\mathbf{s} = (1, 1, 1, 1, 1, 1)$ point for $\{nlj\}$ and $\{\Omega[Nn_z\Lambda]\}$. As shown in Fig 8, one can note that the changing trends of the standard deviations are similar for neutrons and protons. For the $\{nl\}$ single-particle levels, there is no obvious change with changing n, l quantum numbers or single-particle energies. For $\{nlj\}$ and $\{\Omega[Nn_z\Lambda]\}$, respectively, it seems that the increasing trends of the energy uncertainties appear with increasing energies or angular momentum j for a given n, for example, $n = 1$. Note that one spherical j mean-field orbital will split into $(j + \frac{1}{2})$ deformed substates, for example, at $\beta_2 = 0.1$. In addition, it was confirmed that the same conclusions should be obtained using the Monte

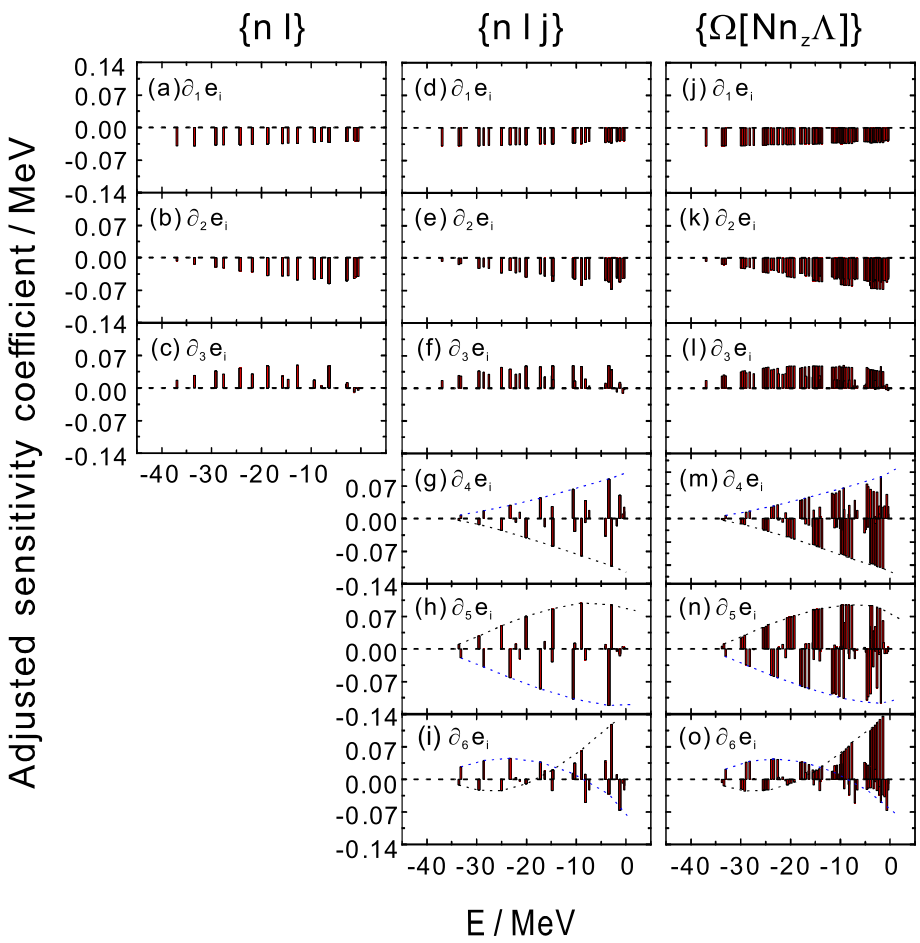

Fig. 7 (Color online) The adjusted sensitivity coefficients $\partial_j e_i$ of the three types of typical neutron single-particle levels labeled by $\{nl\}$, $\{nlj\}$, and $\{\Omega[Nn_z\Lambda]\}$ in ^{208}Pb. See the text for more details

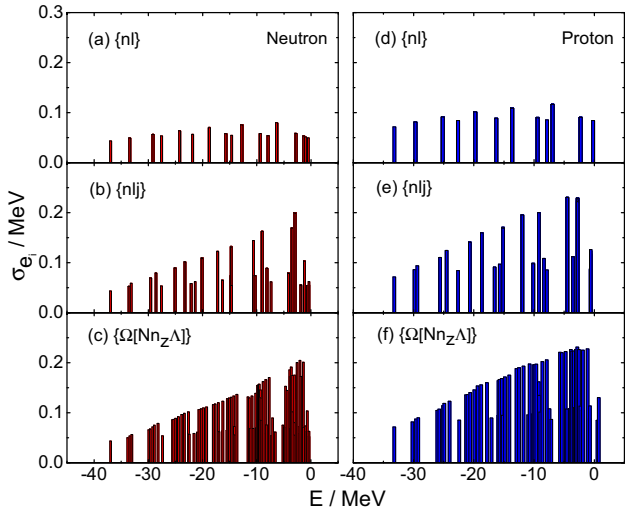

Fig. 8 (Color online) The standard deviation σ_{e_i} of three kinds of typically single neutron (left) and proton (right) energies in ^{208}Pb

Carlo technique. More attention has been paid to the uncertainty propagation from the model parameter rather than the physical discussion behind it.

3.4 Correlation coefficients between single-particle energies

As mentioned above, the single-particle levels are usually the input quantities in further theoretical calculations (e.g., [64, 65]), for example, the calculations of high-K isomers, shell correction, and pairing correction. Both the energy uncertainties and the correlation effects are important for further uncertainty predictions. Based on Eq. 13 the Pearson's correlation coefficients will be able to be calculated between any two levels. Further, we can investigate the correlation effects among them within the 'small' energy domains associated with parameter uncertainties, $\{\sigma_p\}$. Figure 9 shows the two-dimensional scatter plots between three pairs of arbitrarily selected $\{nlj\}$ single-neutron energies, $1i_{13/2} \oplus 1j_{15/2}$, $1i_{13/2} \oplus 3p_{1/2}$, and $1g_{7/2} \oplus 1i_{13/2}$, near the Fermi surface. From the left to right side in this figure, the calculations are applied at $\mathbf{s} = (1,0,0,0,0,0)$, $(1,1,0,0,0,0)$, $(1,1,1,0,0,0)$, $(1,1,1,1,0,0)$, $(1,1,1,1,1,0)$, and $(1,1,1,1,1,1)$ points, respectively. It should be noted that similar to the operation shown in the plot in Fig. 2, before plotting, the normal distributions of the selected single-particle levels

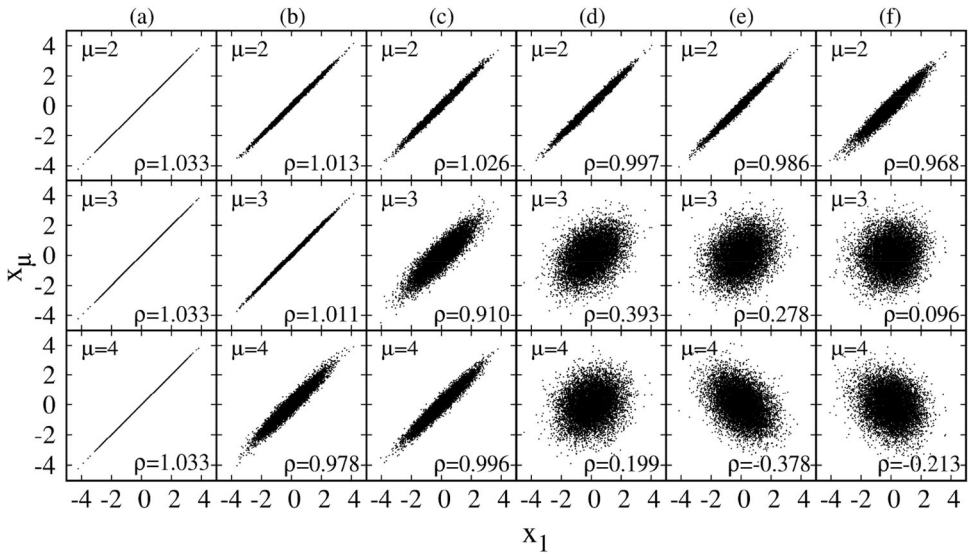

Fig. 9 (Color online) Scatter plots (with correlation coefficients ρ) between three pairs of arbitrarily selected single-neutron energies, $1i_{13/2} \oplus 1j_{15/2}$ (top), $1i_{13/2} \oplus 3p_{1/2}$ (middle), and $1g_{7/2} \oplus 1i_{13/2}$ (bottom), near the Fermi surface in ^{208}Pb. From left to right, the uncertainties of an increasing number of parameters are considered as indicated in the text

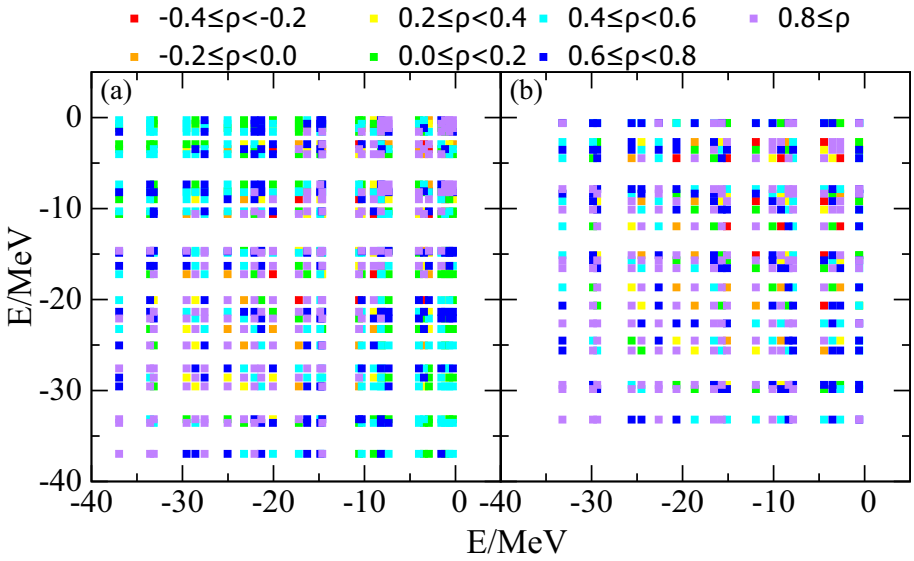

Fig. 10 (Color online) Color-coded plot of the calculated correlation coefficients between single-particle energy levels for neutrons (**a**) and protons (**b**) in ^{208}Pb

are transferred into the standard normal distributions by defining a dimensionless parameter, $x_i = [e_i(\boldsymbol{p}) - e_i(\boldsymbol{p}^{\mathrm{o}})]/\sigma_{e_i}$. In Fig. 9, the dimensionless parameters x_μ for $\mu = 1, 2, 3$, and 4 correspond to the spherically mean-field single-particle levels $1i_{13/2}, 1j_{15/2}, 3p_{1/2}$, and $1g_{7/2}$. When revealing an increasing number of uncertainty parameters, the evolutions of the correlation coefficients and the scatterplot distributions can clearly be seen. In particular, it was found that positive, zero, and negative values appear in the correlation coefficients.

To provide an overall investigation, we show the color-coded plot of the calculated correlation coefficients between single-particle levels with energy $e_i < 0$ for protons and neutrons in Fig. 10. As shown, the correlation coefficients do not have the same values but cover a rather wide range. It is certainly important to consider these correlation effects when the single-particle levels with energy uncertainties are taken as input data to conduct further calculations.

4 Summary

Taking the ^{208}Pb nucleus as the carrier, we investigated the single-particle energy uncertainties and statistical correlations of different levels owing to the uncertainty propagation of independent model parameters, which are important for further theoretical predictions, for example, a K isomer calculation. The adjusted sensitivity coefficients were introduced and discussed for three types of single-particle levels. In addition, the overall standard deviations

of the single-particle levels in the Woods–Saxon nuclear mean field were shown, and the evolution properties were briefly discussed. It was also found that the correlation coefficients involve a rather wide domain, which are important for further theoretical uncertainty predictions relying on single-particle levels. Note that the practical energy uncertainties will depend on the practical standard deviations of the model parameters during the further calculations, whereas the evolution laws of parameter uncertainty propagations and the correlation properties of single-particle levels are still similar and valid. In a follow-up study, we will further investigate the uncertainty propagation of the model parameters with partial correlation effects. It will also be interesting to extend this study to other phenomenological or self-consistent models used in nuclear physics, or even in other fields.

Authors contributions All authors contributed to the study conception and design. Material preparation, data collection and analysis were performed by Zhen-Zhen Zhang, Hai-Yan Meng and Min-Liang Liu. The first draft of the manuscript was written by Hua-Lei Wang and all authors commented on previous versions of the manuscript. All authors read and approved the final manuscript.

References

1. F. Wilczek, Quantun chromodynamics: the modern theory of the strong interaction. Nucl. Par. Sci. **32**, 177 (1982). https://doi.org/10.1146/annurev.ns.32.120182.001141
2. M. Bender, P.H. Heenen, P.G. Reinhard, Self-consistent mean-field models for nuclear structure. Rev. Mod. Phys. **75**, 121 (2003). https://doi.org/10.1103/RevModPhys.75.121
3. M.L. Gorelik, M.G. Uri, A partially self-consistent phenomenological nuclear mean field. Bull. Russ. Acad. Sci. Phys. **76**, 863 (2012). https://doi.org/10.3103/S1062873812080126
4. S.G. Nilsson, C.F. Tsang, A. Sobiczewski et al., On the nuclear structure and stability of heavy and superheavy elements. Nucl. Phys. A **131**, 1 (1969). https://doi.org/10.1016/0375-9474(69)90809-4
5. J. Dudek, W. Nazarewicz, T. Werner, Discussion of the improved parametrisation of the Woods–Saxon potential for deformed nuclei. Nucl. Phys. A **341**, 253 (1980). https://doi.org/10.1016/0375-9474(80)90312-7
6. S. Cwiok, J. Dudek, W. Nazarewicz et al., Single-particle energies, wave functions, quadrupole moments, and g-factors in an axially deformed Woods–Saxon potential with applications to two-sentre-type nuclear problems. Comput. Phys. Commun. **46**, 379 (1987). https://doi.org/10.1016/0010-4655(87)90093-2
7. S. Goriely, N. Chamel, J.M. Pearson, Skyrme–Hartree–Fock–Bogoliubov nuclear mass formulas: crossing the 0.6 MeV accuracy threshold with microscopically deduced pairing. Phys. Rev. Lett. **102**, 152503 (2009). https://doi.org/10.1103/PhysRevLett.102.152503
8. S. Goriely, S. Hilaire, M. Girod et al., First Gogny–Hartree–Fock–Bogoliubov nuclear mass model. Phys. Rev. Lett. **102**, 242501 (2009). https://doi.org/10.1103/PhysRevLett.102.242501
9. M. Bender, K. Rutz, P.-G. Reinhard et al., Shell structure of superheavy nuclei in self-consistent mean-field models. Phys. Rev. C **60**, 034304 (1999). https://doi.org/10.1103/PhysRevC.60.034304
10. A. Savitzky, M.J.E. Golay, Smoothing and differentiation of data by simplified least squares procedures. Anal. Chem. **36**, 1627 (1964). https://doi.org/10.1021/ac60214a047
11. E.B. Wilson, M.M. Hilferty, The distribution of chi-square. Proc. Natl. Acad. Sci. U. S. A. **17**, 684 (1931). https://doi.org/10.1073/pnas.17.12.684
12. K. Levenberg, A method for the solution of certain non-linear problems in least squares. Q. Appl. Math. **2**, 164 (1944). https://doi.org/10.1090/qam/10666
13. D. Benzaid, S. Bentridi, A. Kerraci et al., Bethe-Weizsäcker semiempirical mass formula coefficients 2019 update based on AME2016. Nucl. Sci. Tech. **31**, 1 (2020). https://doi.org/10.1007/s41365-019-0718-8
14. I. Dedes, J. Dudek, Predictive power of theoretical modeling of the nuclear mean-field: examples of improving predictive capacities. Phys. Scr. **93**, 044003 (2018). https://doi.org/10.1088/1402-4896/aab085
15. J. Dobaczewski, W. Nazarewicz, P.-G. Reinhard, Error estimates of theoretical models: a guide. J. Phys. G: Nucl. Part. Phys. **41**, 074001 (2014). https://doi.org/10.1088/0954-3899/41/7/074001
16. I. Dedes, J. Dudek, Propagation of the nuclear mean-field uncertainties with increasing distance from the parameter adjustment zone: applications to superheavy nuclei. Phys. Rev. C **99**, 054310 (2019). https://doi.org/10.1103/PhysRevC.99.054310
17. H.L. Lü, D. Boilley, Y. Abe, C.W. Shen, Synthesis of superheavy elements: uncertainty analysis to improve the predictive power of reaction models. Phys. Rev. C **94**, 034616 (2016). https://doi.org/10.1103/PhysRevC.94.034616
18. C.X. Yuan, Uncertainty decomposition method and its application to the liquid drop model. Phys. Rev. C **93**, 034310 (2016). https://doi.org/10.1103/PhysRevC.93.034310
19. M. Liu, Y. Gao, N. Wang, Statistical errors in Weizsacker–Skyrme mass model. Chin. Phys. C **41**, 114101 (2017). https://doi.org/10.1088/1674-1137/41/11/114101
20. P.-G. Reinhard, W. Nazarewicz, Information content of the low-energy electric dipole strength: correlation analysis. Phys. Rev. C **87**, 014324 (2013). https://doi.org/10.1103/PhysRevC.87.014324
21. B.S. Cai, G.S. Chen, J.Y. Xu et al., α decay half-life estimation and uncertainty analysis Phys. Rev. C **101**, 054304 (2020). https://doi.org/10.1103/PhysRevC.101.054304
22. C.X. Yuan, Y.L. Ge, M.L. Liu et al., Recent shell-model investigation and its possible role in nuclear structure data study. EPJ Web Conf **239**, 04002 (2020). https://doi.org/10.1051/epjconf/202023904002
23. J. Piekarewicz, W.C. Chen, F.J. Fattoyev, Information and statistics: a new paradigm in theoretical nuclear physics. J. Phys. G Nucl. Part. Phys. **42**, 034018 (2015). https://doi.org/10.1088/0954-3899/42/3/034018
24. Q.Z. Chai, W.J. Zhao, M.L. Liu et al., Calculation of multidimensional potential energy surfaces for even-even transuranium nuclei: systematic investigation of the triaxiality efiect on the flssion barrier. Chin. Phys. C **42**, 054101 (2018). https://doi.org/10.1088/1674-1137/42/5/054101
25. Q. Yang, H.L. Wang, M.L. Liu et al., Characteristics of collectivity along the yrast line in even-even tungsten isotopes. Phys. Rev. C **94**, 024310 (2016). https://doi.org/10.1103/PhysRevC.94.024310
26. H.F. Li, H.L. Wang, M.L. Liu, Nuclear collectivity in the even-even $^{164-178}$Yb along the yrast line. Nucl. Sci. Tech. **30**, 100 (2019). https://doi.org/10.1007/s41365-018-0536-4
27. Q.Z. Chai, W.J. Zhao, H.L. Wang et al., Possible observation of shape-coexisting configurations in even-even midshell isotones with N = 104: a systematic total Routhian surface calculation.

Nucl. Sci. Tech. **29**, 38 (2018). https://doi.org/10.1007/s41365-018-0381-5
28. P. Möller, R. Bengtsson, B.G. Carlsson et al., Axial and reflection asymmetry of the nuclear ground state. At. Data Nucl. Data Tables **94**, 758 (2008). https://doi.org/10.1016/j.adt.2008.05.002
29. W. Nazarewicz, R. Wyss, A. Johnson, Structure of superdeformed bands in the $A \approx 150$ mass region. Nucl. Phys. A **503**, 285 (1989). https://doi.org/10.1016/0375-9474(89)90238-8
30. M.J.A. de Voigt, J. Dudek, Z. Szymański, High-spin phenomena in atomic nuclei. Rev. Mod. Phys. **55**, 949 (1983). https://doi.org/10.1103/RevModPhys.55.949
31. F.R. Xu, W. Satuła, R. Wyss, Quadrupole pairng interaction and signature inversion. Nucl. Phys. A **669**, 119 (2000). https://doi.org/10.1016/s0375-9474(99)00817-9
32. F.J. Fattoyev, J. Piekarewicz, Accurate calibration of relativistic mean-field models: correlating observables and providing meaningful theoretical uncertainties. Phys. Rev. C **84**, 064302 (2011). https://doi.org/10.1103/PhysRevC.84.064302
33. P.-G. Reinhard, W. Nazarewicz, Information content of a new observable: the case of the nuclear neutron skin. Phys. Rev. C **81**, 051303 (2010). https://doi.org/10.1103/PhysRevC.81.051303
34. F.J. Fattoyev, J. Piekarewicz, Neutron skins and neutron stars. Phys. Rev. C **88**, 015802 (2012). https://doi.org/10.1103/PhysRevC.86.015802
35. P.R. Bevington, D.K. Robinson, Data reduction and error analysis for the physical sciences. Comput. Phys **7**, 415 (1993). https://doi.org/10.1063/1.4823194
36. D. Rochman, A.J. Koning et al., Nuclear data uncertainty propagation: total Monte Carlo vs. covariances. J. Korean Phys. Soc. **59**, 1236 (2011). https://doi.org/10.3938/jkps.59.1236
37. D. Rochman, S.C. van der Marck, A.J. Koning et al., Uncertainty propagation with fast Monte Carlo techniques. Nucl. Data Sheets **118**, 367 (2014). https://doi.org/10.3938/jkps.59.1236
38. A. Sciacchitano, B. Wieneke, PIV uncertainty propagation. Meas. Sci. Technol. **27**, 084006 (2016). https://doi.org/10.1088/0957-0233/27/8/084006
39. N. Metropolis, S. Ulam, The Monte Carlo method. J. Am. Stat. Assoc. **44**, 335 (1949). https://doi.org/10.2307/2280232
40. J.M. Hammersley, D.C. Handscomb, G. Weiss, Monte Carlo methods. Phys. Today **18**, 55 (1965). https://doi.org/10.1063/1.3047186
41. G.H. Lang, C.W. Johnson, S.E. Koonin et al., Monte Carlo evaluation of path integrals for the nuclear shell model. Phys. Rev. C **48**, 1518 (1993). https://doi.org/10.1103/PhysRevC.48.1518
42. D.J. Dean, M.T. Ressell, M. Hjorth-Jensen et al., Shell-model Monte Carlo studies of neutron-rich nuclei in the 1s–0d-1p-0f shells. Phys. Rev. C **59**, 5 (1999). https://doi.org/10.1103/PhysRevC.59.2474
43. S.E. Koonin, D.J. Dean, K. Langanke, Shell model Monte Carlo methods. Phys. Rep. Rev. Sec. Phys. Lett. **278**, 1 (1997). https://doi.org/10.1016/S0370-1573(96)00017-8
44. G. Marsaglia, W. Tsang, The ziggurat method for generating random variables. J. Stat. Softw. **5**, 1 (2000). https://doi.org/10.18637/jss.v005.i08
45. W. Hörmann, J. Leydold, Continuous random variate generation by fast numerical inversion. ACM trans. Model. Comput. Simul. **13**, 347 (2003). https://doi.org/10.1145/945511.945517
46. C.S. Wallace, Fast pseudorandom generators for normal and exponential variates. ACM Trans. Math. Softw. **22**, 119 (1996). https://doi.org/10.1145/225545.225554
47. G. Box, M. Muller, A note on the generation of random normal deviates. Ann. Math. Statist. **29**, 610 (1958). https://doi.org/10.1214/aoms/1177706645
48. D.-U. Lee, J.D. Villasenor, W. Luk et al., A hardware Gaussian noise generator using the Box-Muller method and its error analysis. IEEE Trans. Comput. **55**, 659 (2006). https://doi.org/10.1109/TC.2006.81
49. A. Alimohammad, S.F. Fard et al., A compact and accurate gaussian variate generator. IEEE Trans. Comput. **16**, 517 (2008). https://doi.org/10.1109/TVLSI.2008.917552
50. E. Boutillon, J.L. Danger, A. Ghazel, Design of high speed a WGN communication channel emulator. Analog Integr. Circuits Process. **34**, 133 (2003). https://doi.org/10.1023/A:1021937002981
51. C.E. Papadopoulos, H. Yeung, Uncertainty estimation and Monte Carlo simulation method. Flow Meas. Instrum. **12**, 291 (2001). https://doi.org/10.1016/S0955-5986(01)00015-2
52. J. Lee Rodgers, W.A. Nicewander, Thirteen ways to examine the correlation coefficient. Am. Stat. **42**, 59 (1988). https://doi.org/10.1080/00031305.1988.10475524
53. K. Pearson, Determination of the coefficient of correlation. Science **30**, 23 (1909). https://doi.org/10.1126/science.30.757.23
54. N. Schwierz, I. Wiedenhöver, A. Volya, Parameterization of the Woods–Saxon potential for shell-model calculations. arXiv:0709.3525 (2007) [nuclth]. 21 Sep 2007
55. J. Dudek, B. Szpak, M.-G. Porquet et al., Nuclear Hamiltonians the question of their spectral predictive power and the associated inverse problem. J. Phys. G Nucl. Part. Phys. **37**, 064031 (2010). https://doi.org/10.1088/0954-3899/37/6/064031
56. D. Wu, C.L. Bai, H. Sagawa, Z.Q. Song, H.Q. Zhang, Contributions of optimized tensor interactions on the binding energies of nuclei. Nucl. Sci. Tech. **31**, 14 (2020). https://doi.org/10.1007/s41365-020-0727-7
57. J. Blomqvist, S. Wahlborn, Shell model calculations in the lead region with a diffuse nuclear potential. Ark. Fys. **16**, 543 (1960).
58. E. Rost, Proton shell-model potentials for lead and the stability of superheavy nuclei. Phys. Lett. B **26**, 184 (1968). https://doi.org/10.1016/0370-2693(68)90335-3
59. V.A. Chepurnov, Average field of neutron and proton shells with $N > 126$ and $Z > 82$. Yad. Fiz. **6**, 955 (1967).
60. J. Dudek, A. Majhofer, J. Skalski et al., Parameters of the deformed Woods-Saxon potential outside $A = 110$–210 nuclei. J. Phys. **65**, 1379 (1979). https://doi.org/10.1088/0305-4616/5/10/014
61. J. Dudek, Z. Szymański, T. Werner, Woods–Saxon potential parameters optimized to the high-spin spectra in the lead region. Phys. Rev. C **23**, 920 (1981). https://doi.org/10.1103/PhysRevC.23.920
62. A. Bhagwat, X. Viñas, M. Centelles et al., Microscopic-macroscopic approach for binding energies with the Wigner-Kirkwood method. Phys. Rev. C **81**, 044321 (2010). https://doi.org/10.1103/PhysRevC.81.044321
63. H.Y. Meng, Y.W. Hao, H.L. Wang et al., Signature of yrast-state structure in even-even hafnium isotopes based on traditional total-routhian-surface calculations and novel E-GOS curves. Prog. Theor. Exp. Phys. **2018**, 103D02 (2018). https://doi.org/10.1093/ptep/pty107
64. D. Naderi, S.A. Alavi, Influence of the shell effects on evaporation residue cross section of superheavy nuclei. Nucl. Sci. Tech. **28**, 161 (2018). https://doi.org/10.1007/s41365-018-0498-6
65. C. Liu, S.Y. Wang, B. Qi et al., Possible candidates for chirality in the odd–odd as isotopes. Chin. Phys. Lett. **37**, 112101 (2020). https://doi.org/10.1088/0256-307X/37/11/112101